Segregation of PIP2 and PIP3 into distinct nanoscale regions within the plasma membrane

Jie Wang and David A. Richards*

Department of Anesthesia, Cincinnati Children's Hospital Medical Center, MLC2001, 3333 Burnet Avenue, Cincinnati, OH 45229, USA

*Author for correspondence (david.richards@cchmc.org)

Biology Open 1, 857–862
doi: 10.1242/bio.20122071
Received 21st May 2012
Accepted 18th June 2012

Summary

PIP_2 and PIP_3 are implicated in a wide variety of cellular signaling pathways at the plasma membrane. We have used STORM imaging to localize clusters of PIP_2 and PIP_3 to distinct nanoscale regions within the plasma membrane of PC12 cells. With anti-phospholipid antibodies directly conjugated with AlexaFluor 647, we found that PIP_2 clusters in membrane domains of 64.5±27.558 nm, while PIP_3 clusters had a size of 125.6±22.408 nm. With two color direct STORM imaging we show that >99% of phospholipid clusters have only one or other phospholipid present. These results indicate that lipid nano-domains can be readily identified using super-resolution imaging techniques, and that the lipid composition and size of clusters is tightly regulated.

Key words: PC12 cell, PIP3, PIP2, Lipid raft

Introduction

Over the last few years the development of super-resolution imaging techniques has begun a revolution in cell biology (Huang et al., 2010). Most subcellular processes occur in regions below the diffraction limit (approximately 200 nm under ideal conditions). Techniques which improve on this include STimulated Emmission Depletion (STED) microscopy which is a point scanning technique like a confocal, but shrinks the focal volume by generated a depleted region around the point of interest to sharpen the resolution (Hein et al., 2008), and Structured Illumination Microscopy (SIM) which analyses the moire interference patterns due to application of non-uniform illumination (Gustafsson et al., 2008). PhotoActivated Light Microscopy (PALM) (Manley et al., 2008) and the conceptually similar Direct Stochastic Optical Reconstruction Microscopy (dSTORM) (Rust et al., 2006) are other widefield super-resolution techniques that are considerably simpler in their equipment requirements. In an appropriate buffer, organic fluorophores can bleach reversibly ("blinking"), which allows a small, random proportion of the fluors in a field to be active at one time. In turn, this allows the localization of individual active fluors to be achieved with very high precision, and repeated cycling of the fluors in a sample allows a very high resolution image to be built up over time.

Lipid rafts are defined as small (10–200 nm) heterogeneous sterol and sphingolipid enriched domains that compartmentalize cellular processes (Pike, 2006). Although their composition varies, one of the lipids often associated with lipid nano-domains is Phosphatidyl Inositol 4,5 Bisphosphate (PIP_2). Signaling through lipid messengers regulates a great many cellular processes (Vanhaesebroeck et al., 2001). Of central importance in many signaling pathways is not only PIP_2, but also Phosphatidyl Inositol 3,4,5 Trisphosphate (PIP_3). PIP_2 and PIP_3 are derived from Phosphatidyl Inositol, and, while they comprise only a small fraction of the membrane, they are responsible for temporal and spatial regulation of many signaling pathways (Di Paolo and De Camili, 2006). This is through the restriction of inositol poly-phosphates to specific sites, and temporally controlled synthesis (reviewed by Krauß and Haucke, 2007). This localized enrichment of PIP_2 and PIP_3 is due to multiple factors, including preferential trapping of the lipids within lipid rafts, binding proteins concentrating PIPs in specific membrane locales, and localized recruitment of enzymes which synthesize PIPs.

A recent study (van den Bogaart et al., 2011) has found that PIP_2 is found in membrane clusters with a size of ~70 nm, where it promotes recruitment of syntaxin through anionic interactions. This process has been reported to depend on the presence of Ca^{2+} ions at micromolar concentrations (Wang et al., 2012). Much less is known about the localization of PIP_3 in cells, although it has been shown to be upregulated at neuronal growth cones (Ménager et al., 2004) and the leading edge of migrating cells (Miao et al., 2011).

In this study, we have used dSTORM to investigate the distribution of PIP_2 and PIP_3 in the plasma membrane of PC12 cells, at a nanoscale resolution (~30 nm). We report that PIP2 and PIP3 are sequestered in separate populations of lipid microdomains, and that the size of the membrane domains that harbor these phospho-inositides differs.

Results and Discussion

Although once thought to consist of a randomly-oriented mixture of proteins and lipids (Singer and Nicolson, 1972), the cellular plasma membrane was subsequently shown to contain lipid clusters (Lee et al., 1974). Initially these were defined biochemically (Brown and Rose, 1992) but over the last 10–20

years a more functional definition has emerged, emphasizing highly-organized lateral domains with distinct molecular components and functional roles (Pike, 2006; Pike, 2009). Phosphatidylinositol(4,5)-bisphosphate PI(4,5)P_2 has been shown to be highly enriched within segregated domains (van den Bogaart et al., 2011), with an apparent size of ~73 nm, roughly the same as the resolution of the STED microscope used in the study. In this work, we sought to further study the distribution of PIP_2 in the plasma membrane, and compare it to the distribution of another poly-phosphorylated phosphoinositide, PIP_3, which is present in the plasma membrane of nerve cells at levels of ~1/6 to 1/2 that of PIP_2 (Goebbels et al., 2010).

In Fig. 1A, we show a representative image of a PC12 cell stained with anti-PIP_2 antibody, an Alexa Fluor 568 anti-mouse secondary, and then deconvolved with a constrained iterative algorithm (SoftWorX from Applied Precision) following 3D acquisition. This illustrates the diffraction barrier for conventional optical imaging. Fig. 1B shows an image from a different cell, where direct STORM is used to localize anti-PIP_2 antibodies directly conjugated with Alexa Fluor 647, to optimize localization precision. The images are at the same scale, and show the huge improvement in detail possible with super-resolution techniques. Analysis of the dimensions of these sub-resolution PIP_2 clusters revealed a tight size distribution with a typical diameter of 64 nm (Fig. 1C). Fig. 1D shows an example of one of the smallest, highly localized particles observed. This has a diameter of 30 nm, indicating an approximate, conservative resolution limit. It is possible that this represents a single antibody with disproportionate labeling, or simply a PIP_2 cluster at the very low end of the size distribution. For comparison, Fig. 1E shows a 3D intensity plot of a PIP_2 cluster with typical size and intensity. This size is consistent with that which has been reported previously for PIP_2 (73 nm) (van den Bogaart et al., 2011) as well as the size of syntaxin clusters in the plasma membrane (68 nm) (Sieber et al., 2007). The localization precision of the STORM system used is approximately 20–25 nm (Rust et al., 2006); consequently the "true" size of these membrane subdomains might be expected to be slightly smaller, around 50–55 nm due to antibodies binding at the edge of lipid domains.

PIP_3 plays a different, but equally important role in cell signaling to PIP_2, and so we repeated our analysis of PC12 cell membranes using an Alexa Fluor 647 direct conjugation of anti-PIP_3 antibodies. Again, widefield imaging provides a resolution impaired view of PIP_3 clusters in the membrane (Fig. 2A) compared to the dSTORM image (Fig. 2B,C). Interestingly, when we analyzed the size distribution of PIP_3 membrane clusters, we found their size was significantly larger (Fig. 2D) (PIP_3 diameter 103±24 nm; $P<0.01$).

In addition to providing greater localization precision, due to the elimination of the additional size burden from the secondary antibody, direct conjugation of the antibodies allowed us to use both PIP_2 and PIP_3 antibodies simultaneously, despite both being monoclonal (i.e. mouse) antibodies. STORM imaging differs from other imaging techniques in that there are essentially no false positives as long as the reporters are sufficiently separated, since only flashing fluors are detected. Consequently there is no auto fluorescence or background. Instead, there is a danger of false negatives (i.e. no signal or very weak signal even when there are antibodies bound). To assess how well we could rely on double labeling experiments, we stained PC12 cells simultaneously with PIP_3 antibodies conjugated to either Alexa Fluor 488, or Alexa Fluor 647. This produced clearly labeled puncta in the membrane (Fig. 3A), of similar size to those seen previously (Fig. 3B). Fig. 3A also shows that the labeling of PIP_3 clusters was not uniform, and the balance between Alexa Fluor 488 labeling and Alexa Fluor 647 labeling is shown in Fig. 3C, on a per cluster basis. When analyzed, this showed that about 70% of the clusters were double labeled (although not necessarily equally), while just over 20% were labeled with AlexaFluor 647 only, and less than 10% were labeled with Alexa Fluor 488. Unlike in conventional optical imaging, the imaged antibodies are close to the size of the resolution used to image them (monoclonal IgG are between 5 and 20 nm depending on axis) (Harris et al., 1995), and so steric crowding becomes an issue when double labeling very small structures. We suspect that this competition between the two antibodies may explain the slightly smaller size of the PIP_3 clusters in these experiments.

When double dSTORM labeling was carried out using PIP_2-Alexa Fluor647 and PIP_3-AlexaFluor488, once again a punctate

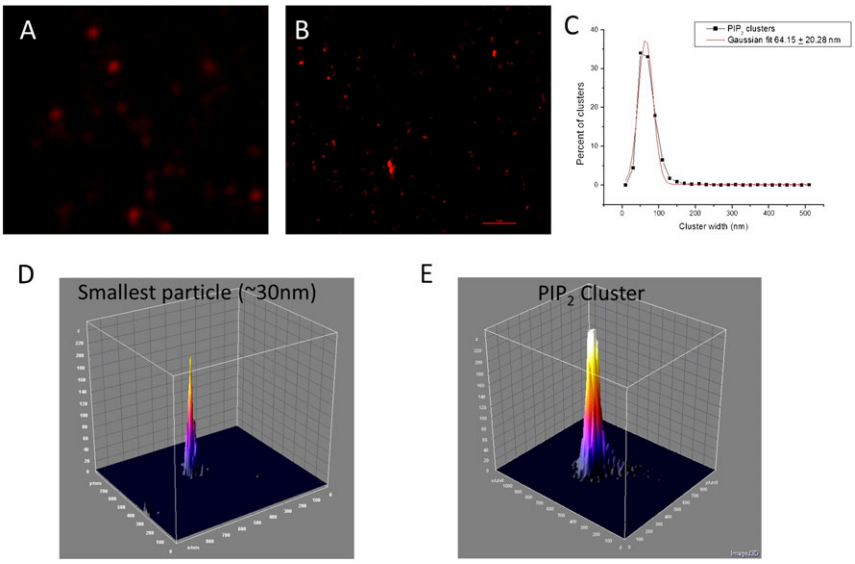

Fig. 1. PIP_2 localizes to 64 nm clusters in the plasma membrane. (**A**) A representative image of a PC12 cell stained with anti-PIP_2 antibody, and an Alexa Fluor 568 anti-mouse secondary. The image was obtained as a 5 micron Z-stack with 100 nm sections, and then deconvolved with a constrained iterative algorithm (SoftWorX from Applied Precision). This illustrates the diffraction barrier for conventional optical imaging. (**B**) A different PC12 cell imaged using dSTORM with anti-PIP_2 antibody directly conjugated to Alexa Fluor 647. A and B are at the same scale, scale bar 1 µm. (**C**) Size distribution of labeled clusters analyzed as Full Width Half Maximum (FWHM) of X and Y Gaussian fits, ($n=1348$ rafts). (**D**) 3D intensity plot of a bright object with amongst the smallest diameter, to illustrate instrument resolution. (**E**) 3D intensity plot of a typical PIP_2 cluster.

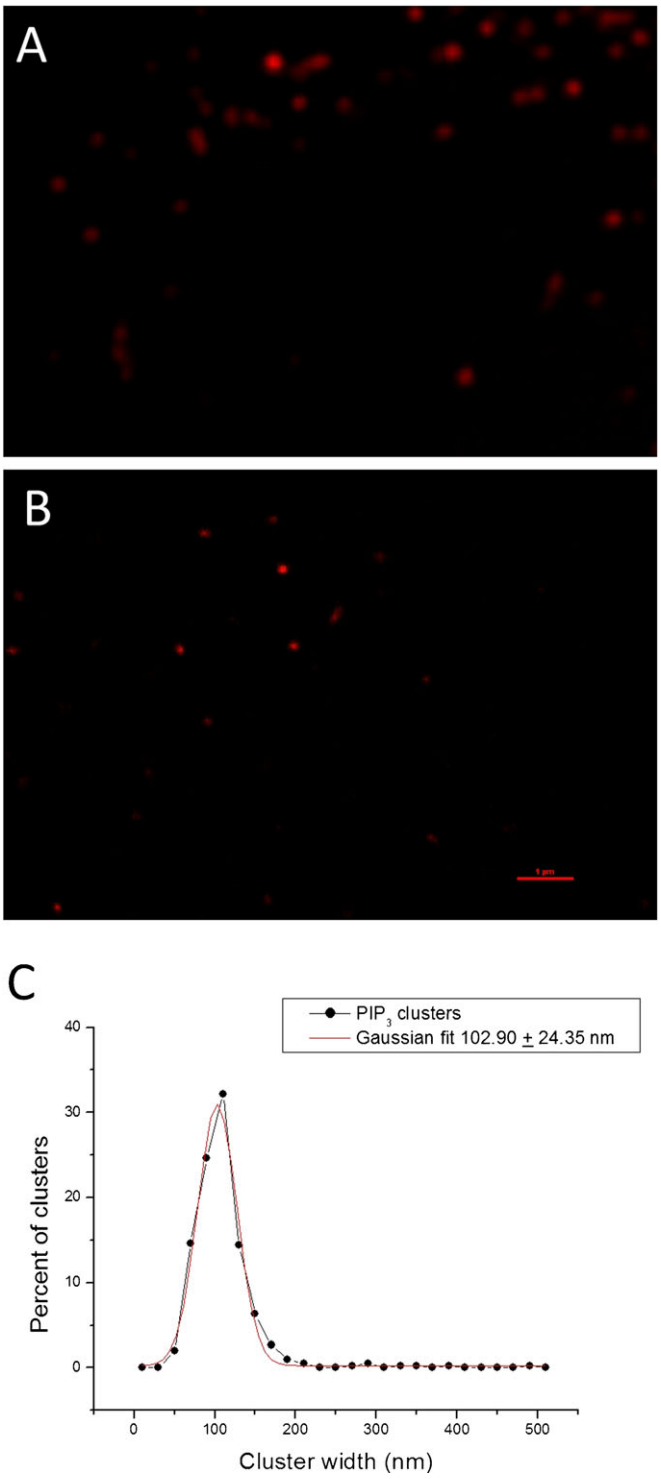

Fig. 2. PIP_3 localizes to 103 nm clusters in the plasma membrane. (**A**) A representative image of a PC12 cell stained with anti-PIP_3 antibody, and an Alexa Fluor 568 anti-mouse secondary. The image was obtained as in Fig. 1A. (**B**) A different PC12 cell imaged using dSTORM with anti-PIP_3 antibody directly conjugated to Alexa Fluor 647. A and B are at the same scale, scale bar 1 µm. (**C**) Size distribution of labeled clusters analyzed as Full Width Half Maximum (FWHM) of X and Y Gaussian fits, (n=796 rafts).

staining pattern was observed (Fig. 4A). Interestingly, very few double labeled puncta were observed. In Fig. 4B we show a zoomed-in image of a double labeled microdomain, with a line profile plot beneath it showing the very good agreement between the two channels. In Fig. 4C we have plotted Alexa488 channel intensity against Alexa Fluor647 intensity as we did in Fig. 3C. Only 8 co-labeled puncta were observed out of 842 analyzed, and these had an average size of 114.4±11 nm with a range from 69 nm to 168 nm. Potentially, the larger average size might indicate that these are co-mingled domains, but further experiments would have to be carried out to investigate that. In Fig. 4D we have analyzed the microdomain size of PIP_2 and PIP_3 clusters from within the same cells, and show that they differ markedly. In widefield images nanoscopic features will tend to be circular, since that is the shape of the PSF convolved spot, but this does not apply to super-resolution images. To perform an initial investigation as to whether the lipid clusters are circular or show more complex morphology, we analyzed the shape of the domains using the roundness index (essentially the ratio of actual area to that resulting from the longest dimension; a circle is therefore 1). As shown in Fig. 4E, we found that both PIP_2 and PIP_3 harboring domains were only moderately circular. The distribution of roundness was not quite the same, however; PIP_2 harboring domains appeared to show a bi-modal distribution containing both circular (28% of clusters) and stretched (72%) clusters. PIP_3 harboring domains showed a broader distribution with a single peak (when analyzed as two populations, >90% fell into the main peak). The differences in the size distributions, the lack of label overlap, and the slight morphological differences, provide convincing evidence that PIP_2 and PIP_3 segregate into different classes of nanoscale lipid domains.

We used the double labeled data to calculate the proportion of the membrane that was decorated by labeling with each antibody, in order to provide a lower estimate for the amount of phopshoinositides found in the membrane. PIP_2 levels in the plasma membrane are typically in the range of 1–3% of total lipid (McLaughlin et al., 2002). In our study, we find that in the dSTORM images, an average of 2.6% of the cell area is occupied by PIP_2 clusters. This implies that PIP_2 is very highly concentrated within clusters, in agreement with a recent report (van den Bogaart et al., 2011) that suggested PIP2 contributed approximately 82% to the inner leaflet lipids within microdomains. PIP_3 is less abundant in the plasma membrane. A recent report using gas chromatography to quantify PIP3 levels in neurons indicates that PIP_3 levels are between half and a sixth of those of PIP_2. In other cells, using perhaps less sensitive techniques, estimates of PIP_3 concentration vary between 1% (Corbin et al., 2004) and 5% (Insall and Weiner, 2001) of the concentration of PIP_2. The clear, distributed signal shown by anti-PIP_3 antibodies in PC12 cells leads us to suspect that PIP_3 levels in PC12 cells are more similar to those seen in neurons, but this remains to be determined experimentally. In terms of area coverage, however, we find that PIP_3 clusters cover more of the surface of the cell (7.1%) than PIP_2. A large part of this is due to the larger size of PIP_3 membrane clusters. This underlines how different the two classes of phosphoinositide microdomains must be. From van den Bogaart et al., there would be predicted to be about 1000 PIP_2 molecules per microdomain (based on headgroup size, and 82% microdomain coverage) (van den Bogaart et al., 2011). The PIP_3 clusters we report here have twice the surface area of PIP_2 clusters, and so even at the highest reported levels of PIP_3, they would have a within raft concentration of less than one fifth that seen in PIP_2 microdomains. Consequently, while PIP_2 may self-assemble

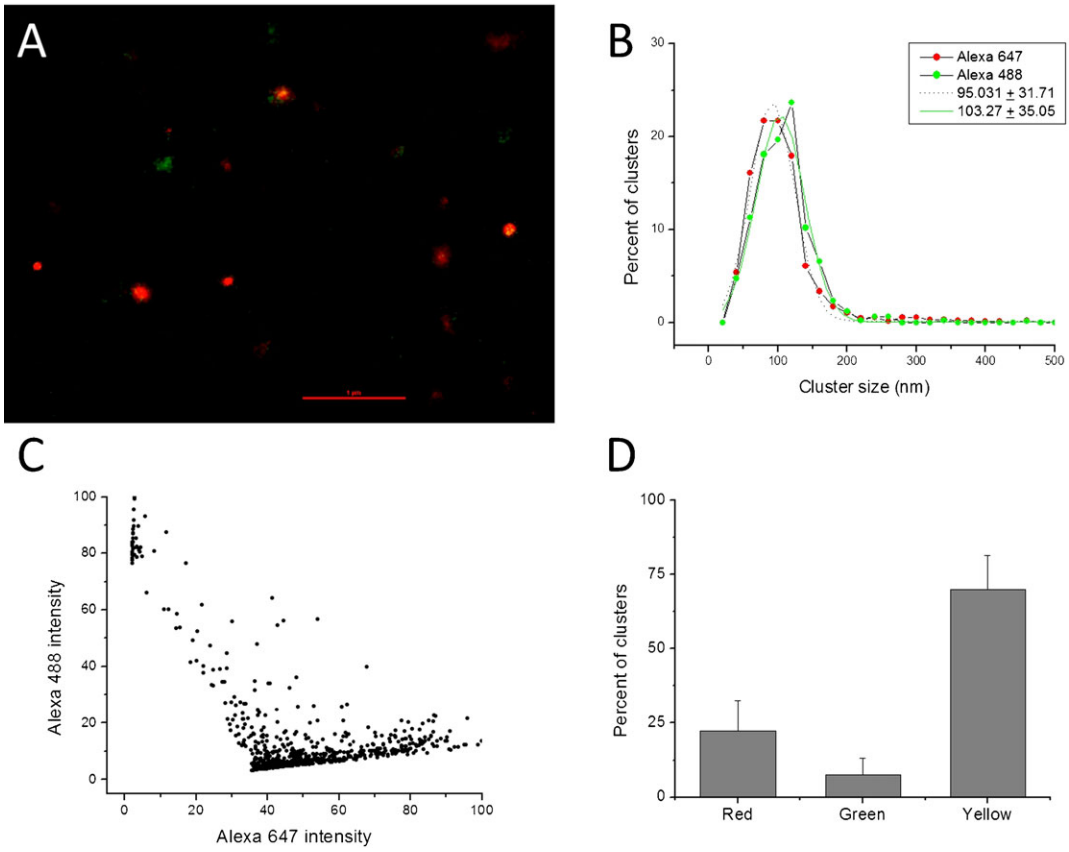

Fig. 3. Testing for detection of co-localization. (**A**) dSTORM image of lipid clusters labeled with anti-PIP_3- Alexa Fluor 488 and anti-PIP_3- Alexa Fluor 647. Scale bar 1 µm. (**B**) Size distribution of labeled clusters analyzed as Full Width Half Maximum (FWHM) of X and Y Gaussian fits, (n=926 rafts). (**C**) Intensity of green and red channels plotted against each other for each raft. (**D**) Comparison of raft fractions labeled with Alexa Fluor 488, Alexa Fluor 647, or both.

into rafts through electrostatic interactions (van den Bogaart et al., 2011), some other mechanism – perhaps recruitment and or retention by protein interactions (McLaughlin and Murray, 2005) – must be responsible for their integrity.

In addition to our biological conclusions, we hope that this manuscript will encourage others to re-address the subcellular localization of other signaling components, by taking advantage of the recent developments in super-resolution microscopy. The three broadly defined categories of super-resolution techniques each have their own strengths. While SIM and STED microscopy are capable of faster acquisition, the stochastic localization techniques (STORM and PALM) offer high localization precision with low background. This can be seen when comparing the PIP_2 clusters described here, with those recently shown by van den Bogaart et al. (van den Bogaart et al., 2011). The size is broadly in agreement (73 nm in the previous report, compared to our finding of 65 nm, well within the margin of error for both techniques), but the signal to noise is dramatically better with STORM. This reflects the confidence resulting from repeated localization of the same fluorophore, the loss of background fluorescence as a result of both the requirement for molecular blinking (not seen in autofluorescence) and the benefits of TIRF excitation.

Materials and Methods

Antibody conjugation

50 µl (1 mg/ml) mouse anti-pip_2 or pip_3 (Echelon Inc) IgG monoclonal antibody were conjugated according to the manufacturer's instructions, with Alexa Fluor 647 carboxylic acid succinimidyl ester and Alexa Fluor 488 carboxylic acid succinimidyl ester (both Invitrogen), at a ratio of around 1–3 dye molecules per molecule of IgG. The conjugated and unconjugated antibodies were separated by NAP-5 gel filtration columns (GE healthcare). These antibodies have been widely used in applications where quantification of PIP_2 (e.g. Leloup et al., 2010) or PIP_3 (e.g. Maffucci et al., 2009) has been carried out in parallel.

Cell staining

PC12 cells (ATCC) were maintained in flasks in F12 medium (Invitrogen) supplemented with 15% horse serum (ATCC) and 2.5% Fetal bovine Serum (Invitrogen). Prior to experiments they were split and seeded into 6 well dishes containing acid-washed, NO. 1.5 Schott glass cover slips (Warner Instruments) previously coated with GelTrex (Invitrogen). For cell staining, cells were fixed on the coverslips in 2% formaldehyde (Sigma) and non-serum medium for 20 minutes, transferred to a new dish, washed three times for 5 minutes in phosphate-buffered saline (PBS, Bio-Rad), and permeabilized in 0.5% Igepal (Sigma) for 15 minutes, washed again and blocked with 10% normal goat serum (Invitrogen), at room temperature for 2 hrs. Then protected from light, the coverslips were incubated with 10 µg/ml of appropriate antibody for one hour at 37℃, washed three times with 0.5% normal goat serum for 10 minutes, and one time with PBS only for 5 minutes, post fixed with 3% formaldehyde and 0.1% glutaraldehyde (Electron microscopy science) at room temperature for 10 minutes, washed again three times with only PBS for 5 minutes, and stored in fresh PBS for 1–4 days prior to imaging.

Imaging

Imaging was carried out on a Nikon Ti-E inverted microscope. Laser excitation (647 nm MPB Communications, set to 100mW; and 488 from a multi-line Melles-Griot Argon-ion laser) was applied via TIRF arm with angle of incidence adjusted to maximize signal-to-noise at the plasma membrane. Images were captured through a 100×1.49Na objective on an Andor iXon X3 EMCCD camera. The region of interest was 256×256 pixels, approximately 40 µm square, which corresponds to a sub region of our PC12 cells, which have typical dimensions of

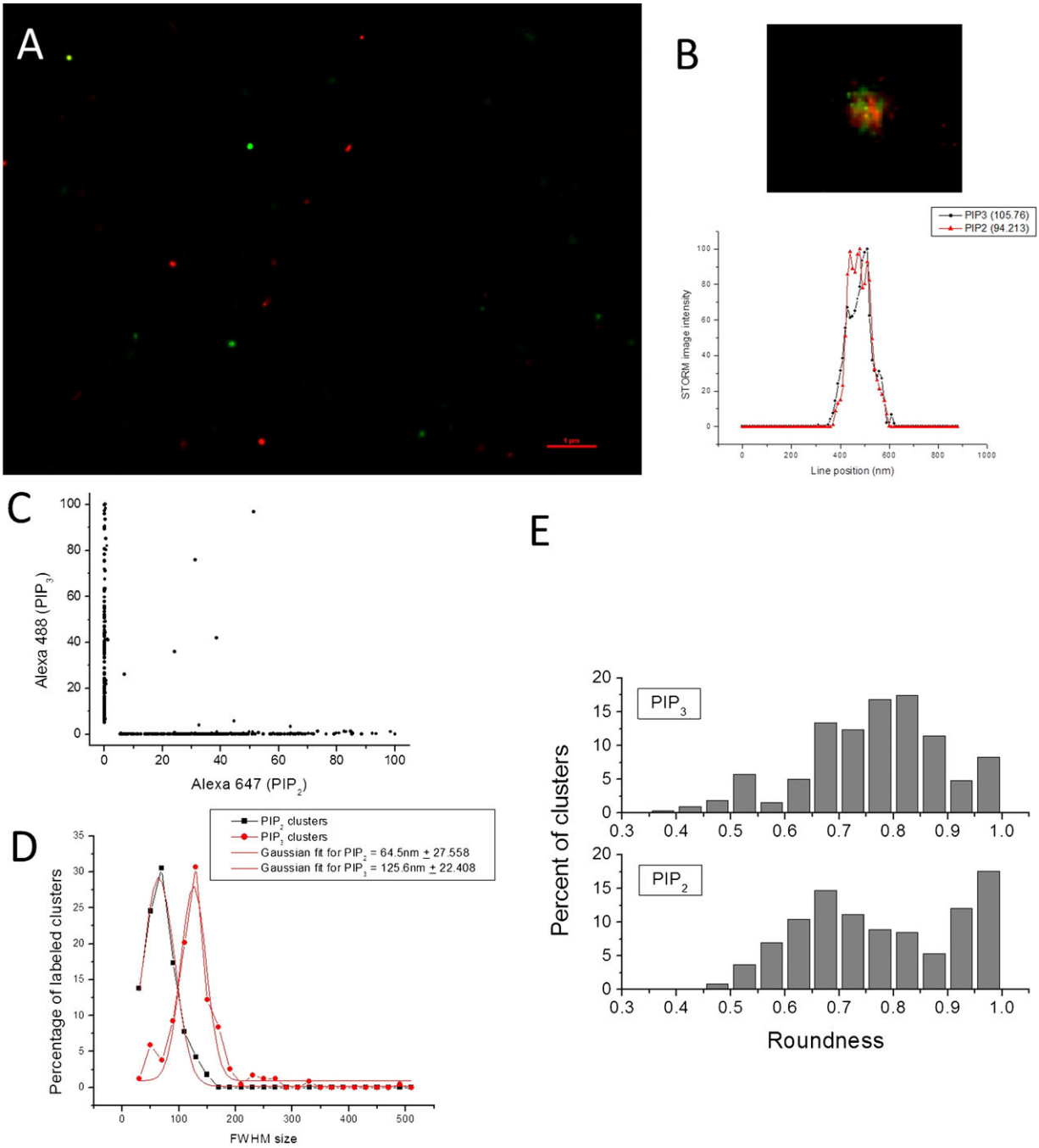

Fig. 4. Almost complete segregation of PIP2 and PIP3 labeling. (**A**) dSTORM image of lipid clusters labeled with anti-PIP_3- Alexa Fluor 488 and anti-PIP_2- Alexa Fluor 647. Scale bar 1 mm. (**B**) Higher magnification image (8-fold) of a rare double-labeled raft, with intensity profiles for the two channels plotted beneath. (**C**) Intensity of green and red channels plotted against each other for each raft. (**D**) Size distribution of labeled clusters analyzed as Full Width Half Maximum (FWHM) of X and Y Gaussian fits, (n=1433 rafts). (**E**) Shape distribution of PIP_2 and PIP_3 harboring domains. The distribution of PIP_2 clusters appears to be bi-modal, while that of PIP_3 clusters is broader, but apparently uni-modal. Data are from 468 (PIP_3) or 521 (PIP_2) domains.

50–80 µm. As a result of the TIRF illumination, signals were restricted to the lower surface of the plasma membrane. Two-dimensional STORM localization was carried out using Nikon elements 3 software, based on the work of Rust et al. (Rust et al., 2006). After rejection of points due to dimness or circularity, around 1–1.5 million molecular localizations were used to form each image channel. The imaging buffer was made to Nikon protocols from Buffer A (10 mM Tris (pH 8.0)+50 mM NaCl), Buffer B (50 mM Tris-HCl (pH 8.0)+10 mM NaCl+10% Glucose), and GLOX (250 µl: 14 mg Glucose Oxidase+50 µl Catalase (17 mg/ml)+200 µl Buffer A) to make MEA imaging buffer (7.0 µl GLOX, 70 µl 1 M MEA and 620 µl Buffer B).

Analysis

STORM images were exported at 10 nm/pixel resolution as JP2000 files. These were opened in ImageJ using the Bio-formats (http://loci.wisc.edu/bio-formats) plugin for ImageJ (NIH). Lipid raft dimensions were measured using Adrian's FWHM plugin (http://rsbweb.nih.gov/ij/plugins/fwhm/index.html). Raft intensities were analyzed as follows. First, a composite grayscale image was created by merging the two channels, to remove selection bias in thresholding. Next, the images were thresholded. Finally, the analyze particle tool in ImageJ was used to convert the spots to individual regions of interest. These ROIs were then imposed on the original green and red channel images to provide the two intensities for each

raft. Roundness was assessed using the shape descriptors plugin for ImageJ: (http://rsb.info.nih.gov/ij/plugins/descriptors.html).

Acknowledgements

We would like to thank Dr. Matt Kofron for helpful comments. This research was supported by National Institutes of Health R01 grant NS054750 (to D.A.R.) and the Department of Anesthesia at CCHMC.

Competing Interests

The authors have no competing interests to declare. The funders had no role in study design, data collection and analysis, decision to publish, or preparation of the manuscript.

References

Brown, D. A. and Rose, J. K. (1992). Sorting of GPI-anchored proteins to glycolipid-enriched membrane subdomains during transport to the apical cell surface. *Cell* **68**, 533-544.

Corbin, J. A., Dirkx, R. A. and Falke, J. J. (2004). GRP1 pleckstrin homology domain: activation parameters and novel search mechanism for rare target lipid. *Biochemistry* **43**, 16161-16173.

Di Paolo, G. and De Camilli, P. (2006). Phosphoinositides in cell regulation and membrane dynamics. *Nature* **443**, 651-657.

Goebbels, S., Oltrogge, J. H., Kemper, R., Heilmann, I., Bormuth, I., Wolfer, S., Wichert, S. P., Möbius, W., Liu, X., Lappe-Siefke, C. et al. (2010). Elevated phosphatidylinositol 3,4,5-trisphosphate in glia triggers cell-autonomous membrane wrapping and myelination. *J. Neurosci.* **30**, 8953-8964.

Gustafsson, M. G., Shao, L., Carlton, P. M., Wang, C. J., Golubovskaya, I. N., Cande, W. Z., Agard, D. A. and Sedat, J. W. (2008). Three-dimensional resolution doubling in wide-field fluorescence microscopy by structured illumination. *Biophys. J.* **94**, 4957-4970.

Harris, L. J., Skaletsky, E. and McPherson, A. (1995). Crystallization of intact monoclonal antibodies. *Proteins* **23**, 285-289.

Hein, B., Willig, K. I. and Hell, S. W. (2008). Stimulated emission depletion (STED) nanoscopy of a fluorescent protein-labeled organelle inside a living cell. *Proc. Natl. Acad. Sci. USA* **105**, 14271-14276.

Huang, B., Babcock, H. and Zhuang, X. (2010). Breaking the diffraction barrier: super-resolution imaging of cells. *Cell* **143**, 1047-1058.

Insall, R. H. and Weiner, O. D. (2001). PIP3, PIP2, and cell movement–similar messages, different meanings? *Dev. Cell* **1**, 743-747.

Krauß, M. and Haucke, V. (2007). Phosphoinositides: regulators of membrane traffic and protein function. *FEBS Lett.* **581**, 2105-2111.

Lee, A. G., Birdsall, N. J., Metcalfe, J. C., Toon, P. A. and Warren, G. B. (1974). Clusters in lipid bilayers and the interpretation of thermal effects in biological membranes. *Biochemistry* **13**, 3699-3705.

Leloup, L., Shao, H., Bae, Y. H., Deasy, B., Stolz, D., Roy, P. and Wells, A. (2010). m-Calpain activation is regulated by its membrane localization and by its binding to phosphatidylinositol 4,5-bisphosphate. *J. Biol. Chem.* **285**, 33549-33566.

Maffucci, T., Raimondi, C., Abu-Hayyeh, S., Dominguez, V., Sala, G., Zachary, I. and Falasca, M. (2009). A phosphoinositide 3-kinase/phospholipase Cgamma1 pathway regulates fibroblast growth factor-induced capillary tube formation. *PLoS ONE* **4**, e8285.

Manley, S., Gillette, J. M., Patterson, G. H., Shroff, H., Hess, H. F., Betzig, E. and Lippincott-Schwartz, J. (2008). High-density mapping of single-molecule trajectories with photoactivated localization microscopy. *Nat. Methods* **5**, 155-157.

McLaughlin, S. and Murray, D. (2005). Plasma membrane phosphoinositide organization by protein electrostatics. *Nature* **438**, 605-611.

McLaughlin, S., Wang, J., Gambhir, A. and Murray, D. (2002). PIP(2) and proteins: interactions, organization, and information flow. *Annu. Rev. Biophys. Biomol. Struct.* **31**, 151-175.

Ménager, C., Arimura, N., Fukata, Y. and Kaibuchi, K. (2004). PIP3 is involved in neuronal polarization and axon formation. *J. Neurochem.* **89**, 109-118.

Miao, B., Skidan, I., Yang, J., You, Z., Fu, X., Famulok, M., Schaffhausen, B., Torchilin, V., Yuan, J. and Degterev, A. (2011) Inhibition of cell migration by PITENINs: the role of ARF6. *Oncogene* [Epub ahead of print].

Pike, L. J. (2006). Rafts defined: a report on the Keystone Symposium on Lipid Rafts and Cell Function. *J. Lipid Res.* **47**, 1597-1598.

Pike, L. J. (2009). The challenge of lipid rafts. *J. Lipid Res.* **50 Suppl**, S323-S328.

Rust, M. J., Bates, M. and Zhuang, X. (2006). Sub-diffraction-limit imaging by stochastic optical reconstruction microscopy (STORM). *Nat. Methods* **3**, 793-796.

Sieber, J. J., Willig, K. I., Kutzner, C., Gerding-Reimers, C., Harke, B., Donnert, G., Rammner, B., Eggeling, C., Hell, S. W., Grubmüller, H. et al. (2007). Anatomy and dynamics of a supramolecular membrane protein cluster. *Science* **317**, 1072-1076.

Singer, S. J. and Nicolson, G. L. (1972). The fluid mosaic model of the structure of cell membranes. *Science* **175**, 720-731.

van den Bogaart, G., Meyenberg, K., Risselada, H. J., Amin, H., Willig, K. I., Hubrich, B. E., Dier, M., Hell, S. W., Grubmüller, H., Diederichsen, U. et al. (2011). Membrane protein sequestering by ionic protein-lipid interactions. *Nature* **479**, 552-555.

Vanhaesebroeck, B., Leevers, S. J., Ahmadi, K., Timms, J., Katso, R., Driscoll, P. C., Woscholski, R., Parker, P. J. and Waterfield, M. D. (2001). Synthesis and function of 3-phosphorylated inositol lipids. *Annu. Rev. Biochem.* **70**, 535-602.

Wang, Y. H., Collins, A., Guo, L., Smith-Dupont, K. B., Gai, F., Svitkina, T. and Janmey, P. A. (2012). Divalent cation-induced cluster formation by polyphosphoinositides in model membranes. *J. Am. Chem. Soc.* **134**, 3387-3395.